

**GRAIN SIZE DISTRIBUTION AFTER SIMILAR AND DISSIMILAR GAS
TUNGSTEN ARC WELDING OF A FERRITIC STAINLESS STEEL****E. Ranjbarnodeh^a, S. Serajzadeh^b, A. H. Kokabi^b, A. Fischer^c**^a Mining and Metallurgical Engineering Department, Amirkabir University of Technology, Tehran, Iran^b Department of Materials Science and Engineering, Sharif University of Technology, Tehran, Iran^c Materials Science and Engineering, University Duisburg-Essen, Duisburg, Germany*(Received 21 May 2012; accepted 27 October 2014)***Abstract**

In this study, gas tungsten arc welding of ferritic stainless steel and grain size distribution in heat affected zone of the welded samples were investigated. Both similar and dissimilar arc welding operations were considered where in dissimilar welding joining of stainless steel to mild steel was examined. In the first stage, a three-dimensional model was developed to evaluate temperature field during and after arc welding while the model was performed using finite element software, ANSYS. Then, the effects of welding heat input and dissimilarity of the joint on the weld pool shape and grain growth in HAZ of stainless steel was investigated by means of model predictions and experimental observations. The results show that the similar joint produces wider HAZ and considerably larger grain size structure while in the dissimilar welds, the low carbon part acts as an effective heat sink and prevents the grain growth in the stainless steel side as well reduces the welding maximum temperature.

Keywords: Welding; HAZ; Modeling; Steels.

1. Introduction

Stainless steels are extensively employed in various industries because of their resistance to corrosion and mechanical properties. One of the main problems during welding of this type of steels, particularly in ferritic stainless steels, is extensive grain growth in heat affected zone HAZ leading to poor toughness in this region. However, the grain growth may be controlled by imposing relatively low heat inputs [1]. In this regard, a few works have been conducted concerning the effect of welding conditions on determination of temperature variations as well as metallurgical events during welding of stainless steels employing both experimental techniques and mathematical modeling. Katsareas and Yostous [2] presented two-dimensional and three-dimensional models to determine temperature variations and residual stresses distribution in a dissimilar joint between A508 and AISI304L. Taban et al. [3] have studied weldability of a high chromium stainless steel in plasma arc welding process where in this work, butt welds were made with and without filler metal and then the produced joints were characterized by the aid of microstructural observations and mechanical testing. Choi and Mazumder [4] have studied gas metal arc welding of austenitic stainless steel AISI

304 using mathematical modeling and welding experiments. Tsoukantas and Chryssolouris [5] have investigated remote welding process of AISI 304 stainless steels employing finite element method in which the effects of the incidence angle of the laser beam on the geometry of weld zone were investigated. Zacharia et al. [6] have proposed a computational model to predict temperature distribution and weld pool geometry in Tungsten arc welding of AISI 304 stainless steels. Lee and Chang [7] have employed a three-dimensional finite element analysis to estimate temperature and residual stress distributions in arc welding of steel parts. McPherson et al. [8] have studied the microstructures and mechanical properties of the weld zone in dissimilar welding of duplex stainless steel to low carbon steel after submerge arc welding process. Satyanarayana et al. [9] have investigated dissimilar friction welding of austenitic to ferritic stainless steels where different aspects including mechanical properties, microstructures, residual stresses, and corrosion resistance of the weld were considered and studied. Lee et al. [10] have used a mathematical model based on the finite element method to predict residual stresses and their distribution after butt welding of stainless steels and carbon steels and also, they have compared and studied the differences in distributions

* Corresponding author: islam_ranjbar@yahoo.com

of residual stresses in these two grades of steels.

Hadadzadeh et al. [11] investigated the heat affected zone (HAZ) softening behavior of strain-hardened Al-6.7Mg alloy welded by gas tungsten arc welding (GTAW) process. They found that increasing the heat input led to formation of a wider HAZ. Moreover, the size of the precipitates was increased at higher heat inputs.

Ranjbarnodeh et al. [12] studied microstructural characteristics of tungsten inert gas (TIG) welded AISI409 ferritic stainless steel. They investigated the effect of the welding parameters on grain size, local misorientation and low angle grain boundaries. They found that the final state of strain is the result of the competition between welding plastic strains and stress relieving from recrystallization but the decisive factor in determining the grain size in HAZ is heat input.

Priadi et al. [13] attempted to calculate a mathematical model for austenite grain growth of 0.028% Nb steel, which can account for abnormal grain growth. The quantitative calculation of austenite grain growth generated from this model fit well with the experimental grain growth data obtained during reheating of niobium steels. The results of this study showed that increasing the temperature increases the austenite grain size, with a sharp gradient observed at higher temperatures.

Zhang et al. [14] studied the grain structure in the heat-affected zone (HAZ) of 12 wt.% Cr ferritic stainless steel under laser + pulsed gas metal arc welding. They used Monte Carlo method to simulate the evolution of grain structure in the HAZ of the ferritic stainless steel. The results showed that the width of coarse grain heat-affected zone and the grain structure varied dramatically along the fusion line direction, the maximum mean grain size near the top surface was much larger than that close to the weld root.

Ohno et al. [15] investigated the effect of the temperature gradient on the grain growth by means of the phase-field simulations. They found that the local grain growth is determined only by the local thermal history regardless of the temperature gradient, and hence, the temperature gradient does not directly influence the local grain growth.

In this study, a three-dimensional model is employed to determine temperature distribution in butt welding of stainless steels in which both similar and dissimilar welding processes are considered. Then, by means of the developed model, the effect of heat input on temperature variations of the materials being welded as well as metallurgical events in the HAZ within the stainless steel side are evaluated. To solve the heat transfer problem, the finite element software, ANSYS is employed. In order to verify the predictions, welding experiments are conducted under different welding conditions then the measured and

the predicted weld pool shapes are compared. Furthermore, grain size distribution in the stainless steel side of the joint is also measured and discussed based on the predicted thermal cycles.

2. Thermal model

In the present study, a mathematical model was employed to determine temperature distribution during and after gas tungsten arc welding process. In order to solve the governing heat conduction problem, finite element software, ANSYS has been utilized where the following equation was used to predict temperature variations within the metal being welded under unsteady state conditions [7].

$$\frac{\partial}{\partial x} \left(k \frac{\partial T}{\partial x} \right) + \frac{\partial}{\partial y} \left(k \frac{\partial T}{\partial y} \right) + \frac{\partial}{\partial z} \left(k \frac{\partial T}{\partial z} \right) = \rho c \frac{\partial T}{\partial t} \quad (1)$$

here, T is the temperature, k the thermal conductivity, c is the specific heat, ρ is the density and t denotes welding time. “ x ”, “ y ” and “ z ” represent welding, transverse and thickness directions, respectively. Convection-conduction boundary conditions as denoted in Eq. (2) were assumed for all surfaces. However, in the region under the welding arc an imposed heat flux of Gaussian type, $q(z,y,t)$, was also considered as illustrated in Eqs. (3) and (4) [16]. It should be noted that the effect of radiation was ignored and instead an effective heat convection coefficient was considered for this above region. The Eqs. (2-4) are given as follows:

$$-k \frac{\partial T}{\partial n} = h(T - T_a) \quad (2)$$

$$-k \frac{\partial T}{\partial z} = h_c(T - T_a) - q(z, y, t) \quad (3)$$

$$q(z, y, t) = \frac{3\eta VI}{\pi r^2} \exp\left(-\frac{3}{r^2}[(z+vt)^2 + y^2]\right) \quad (4)$$

where “ n ” represents the normal direction to the surface boundary, T_a denotes the ambient temperature, $q(r)$ is the welding input energy, “ h ” is convection heat transfer coefficient, “ h_c ” is the effective convection heat transfer for the region under welding arc, V is welding voltage, I is welding current, and “ r ” is the Gaussian distribution parameter taken as 1.5 mm. “ η ” describes arc efficiency and this factor was assumed as 0.60 [17].

In the numerical solution of the above problem, a concentrated high heat flux is imposed to the sample, or in other words, a severe thermal gradient is formed in the central region of the weldment at the positions close to the welding arc, so very fine elements are required in the region of weld zone and HAZ to accurately predict thermal response of the material. Therefore, the adaptive mesh system was employed in

which the size of the elements increases at the distances far enough from the weld centerline as displayed in Figure 1. As a part of finite element analysis, mesh sensitivity analysis was also carried out to evaluate the effect of mesh density on the model results. The maximum temperature in the weld pool was taken as the convergence condition and the analysis was performed for different numbers of elements in the arc region until this temperature tend to a constant value. As a result, based on the employed mesh sensitivity procedure, 17100 eight-node elements and 21385 nodes have been used in the construction of the mesh system where three dimensional thermal elements i.e. SOLID70, were used for the bulk material and the surface elements of the type of SURF152 were utilized to handle the imposed surface heat flux. In the model, the welding operation was divided into three stages including heating, welding, and cooling steps, where a small fraction of the total time was allocated to the heating and welding stages while a significant part was assigned for cooling to the room temperature. Besides, the magnitudes of convection heat transfer coefficients were taken as 15 W/m²K for the surfaces in contact with the air and 800, 1100 W/m².K for the surfaces in contact with the backing plate and fixtures, and the region below the welding arc, respectively [18]. Heat transfer due to fluid flow in the weld pool was considered by increasing the thermal conductivity above the melting temperature by the factor of three [19]. The thermal conductivities of the stainless steel at different temperatures are listed in Table 1, while

the specific heat of the stainless steel part was taken as 460 J/kg.K in all temperatures. It should be noted that the influence of dilution on heat transfer in dissimilar welding process was also considered in the model. This effect was considered by changing material properties in the weld zone using MPCHG command in ANSYS. This command changes the material number of the specified elements between load steps in solution part of analysis. At each stage of solution, the temperature distribution of model was checked and the melted part of the joint was determined by selecting the elements with temperatures higher than the melting point for carbon steel and stainless steel. Then, the material properties of these elements were changed to the new material number using lever rule.

Table 1. Thermal conductivity of the stainless steel

Temperature (°C)	Thermal Conductivity (W/m.K)
20	25
500	30
1400	30
2000	90

3. Experimental

Welding of ferritic stainless steel (AISI409) and low carbon steel (CK4) were examined and both similar and dissimilar joining experiments were carried accordingly. The chemical compositions of the steels are listed in Table 2. The samples with

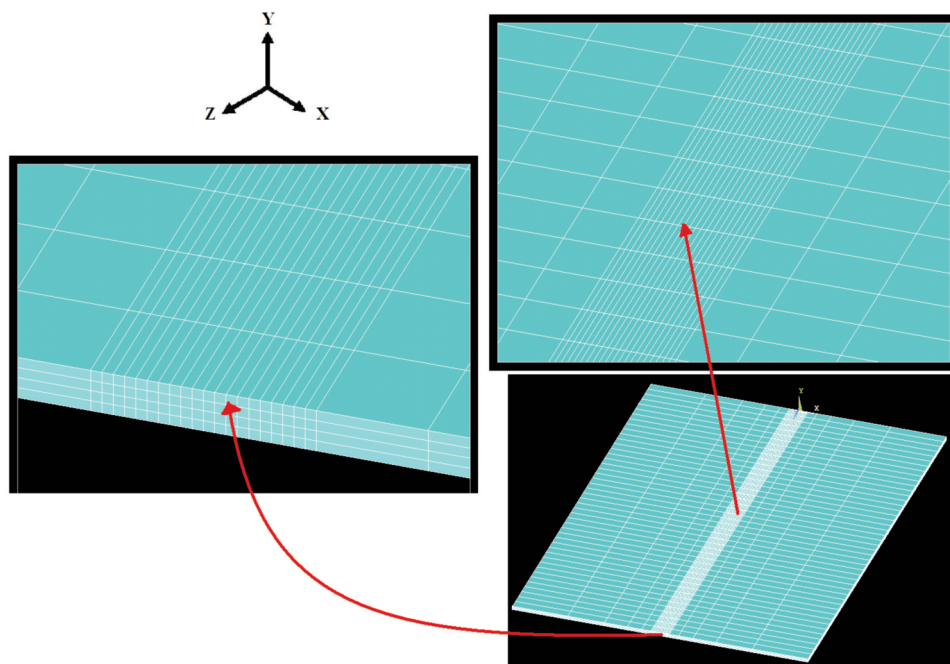


Figure 1. The mesh system used in the model.

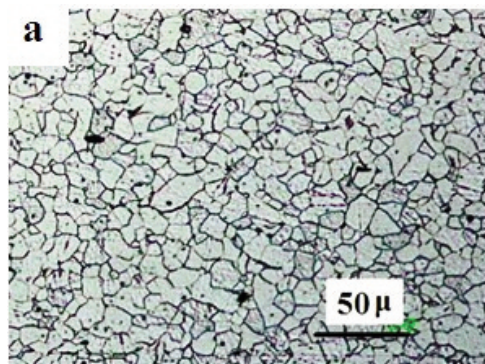
dimensions of $(0.002 \times 0.8 \times 0.45) \text{ m}^3$ were welded using automatic TIG welding machine in which no filler metal was used. The diameter of tungsten electrode and arc length was 1.6 and 1 mm, respectively. Six samples, including three similar and three dissimilar joints, were prepared and edged cleaned before welding process. In these experiments, different welding currents were selected to investigate the effect of heat input on grain size distribution in HAZ in the stainless steel. Table 3 presents the parameters used in the welding experiments. After the process of joining, a macro section at middle of the weld line was prepared from each sample and the weld pool geometry and HAZ were determined. The metallographic samples were also prepared by Vilella's reagent containing 1 g picric acid, 100 ml ethanol, 5 ml hydrochloric acid with the etching duration of 35 s. Finally, the grain size distribution in HAZ and the mean grain size of base metal of stainless steel part was determined.

Table 2. Chemical compositions of the samples

Steel	C	Si	Mn	Ni	Cr	Ti	S	P
1.4512 (AISI409)	0.015	0.59	0.27	0.13	11.28	0.17	0.0095	0.022
1.1005 (CK4)	0.025	0.013	0.19	0.04	0.01	-	0.0034	0.015

Table 3. Welding parameters used in experiments

Sample	Welding speed (mm/s)	Welding current (A)	Joint type
S1	3.56	105	Dissimilar
S2	3.56	120	Dissimilar
S3	3.56	135	Dissimilar
S4	3.56	105	Similar
S5	3.56	120	Similar
S6	3.56	135	Similar



4. Results and discussion

The initial microstructures of the used steels are shown in Figure 2. As can be seen, both steels have ferritic structure. Due to the presence of titanium, the stainless steel contains carbo-nitrides as the second phase, i.e. black fine regions shown in Figure 2b. Besides, the mean grain sizes of the stainless and carbon steels were also calculated as 45 and 15 μm, respectively.

Figure 3 compares the predicted and the real weld pool geometries for similar and dissimilar welding processes, i.e. samples S2 and S5. A reasonable consistency between the predictions and experimental observations can be noticed. Furthermore, large grains of order of 400 μm, both in the weld zone and in the HAZ, have been produced after similar welding, while much smaller grains have been formed in the dissimilar welding.

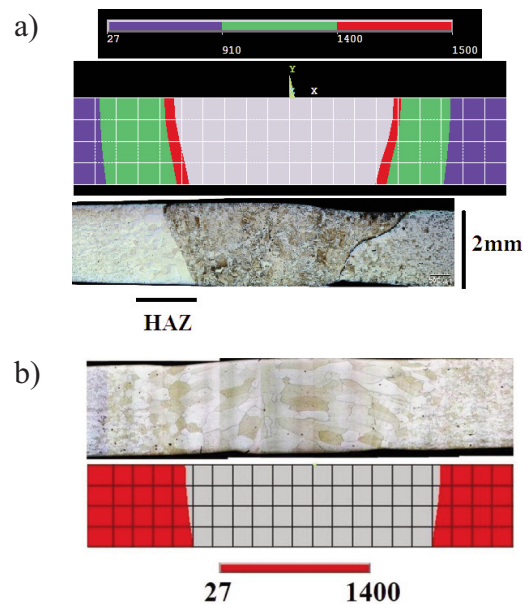


Figure 3. Comparison between the predicted and the measured weld pools for, a) sample S2, b) sample S5.

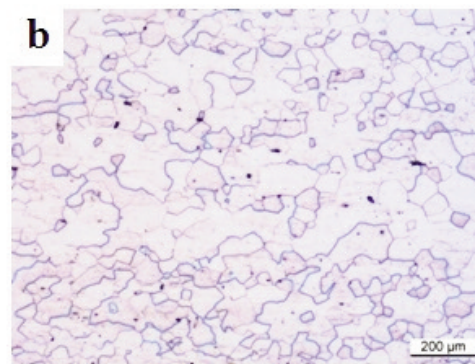


Figure 2. The microstructures of the steels a) low carbon steel, b) ferritic stainless steel.

Figure 4 also shows the micrographs of the grain size distribution in the stainless steel for different similar welded samples. Very large grain size variations are observed in the welded stainless steel, particularly for the welding current of 135 A. However, the grain growth is controlled during dissimilar welding as shown in Figure 3b. That phenomenon may be attributed to the imposed thermal cycles during and after welding operation and it can be evaluated by the model predictions, as given in Figure 5. This figure shows temperature distribution in dissimilar and similar joints under the welding current of 120A. As can be seen, dissimilar joint has a smaller weld pool. It may be due to the effect of carbon steel part in dissimilar welded sample with higher thermal diffusivity acting as a heat an effective sink and consequently the higher amount of the imposed heat is transferred through this side.



Figure 4. The effect of welding current on the weld pool shape of the similar joints, a) sample S6, b) sample S4.

Accordingly, it is expected that smaller heat affected zone would be formed in dissimilar welding, as shown in Figure 6. Figure 7 also presents the temperature cycles at the different points of welded plate for samples S2 and S5 in the stainless part of the joint. As seen in the figure, the similar joint undergoes higher peak temperature and longer heating duration compared to the other sample that can result in coarser grain size distribution.

The effect of welding current on the grain size distribution in HAZ for similar and dissimilar joints is shown in Figure 8. The higher welding current, i.e. high heat input conditions, leads to larger weld pool with very coarse grain sizes or order of 400 μm for similar joints and 200 μm for the dissimilar joints. Even, the presence of carbo-nitrides due to addition of titanium could not prevent extensive grain growth within the ferritic stainless steel. Thus, the control of heat input and selecting the optimum welding current is of importance particularly in similar welding of the employed ferritic stainless steel which is more susceptible to grain growth. The thermal model and its results can be used as a guideline in selecting an appropriate welding current. For instance, Figure 9 shows the penetration depth of weld pool as a function

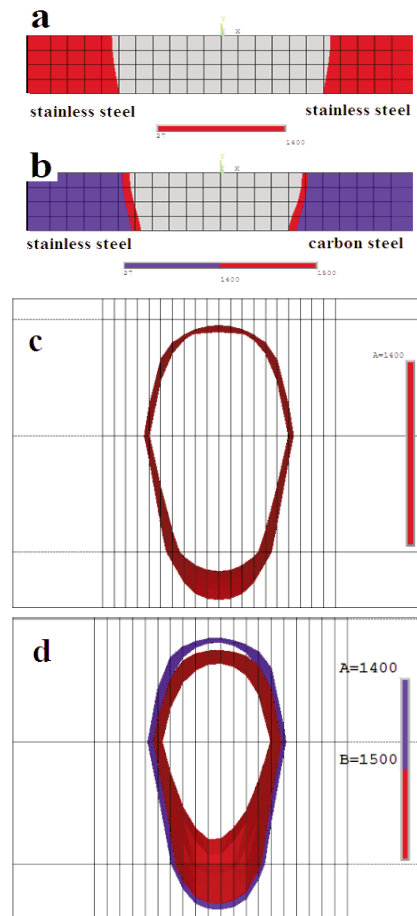


Figure 5. The predicted temperature distributions at the middle of the plate being welded a) sample S5 (front view), b) sample S2 (front view), c) sample S5 (top view) and sample S2 (top view).

of welding current, and the current about 95A seems to be an appropriate one to achieve full penetration, as well as to impose the smallest amount of heat input.

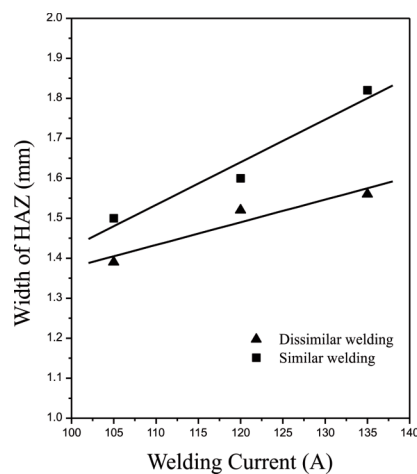


Figure 6. The effect of welding current on the width of HAZ.

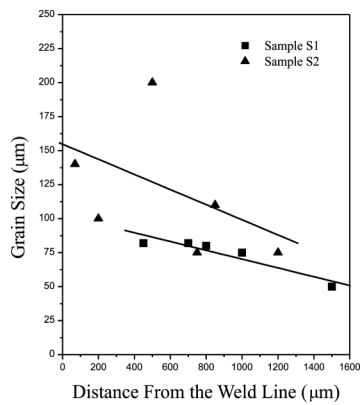


Figure 7. Temperature cycles of the samples S2 and S5 in the of $x=0, 3, 5$ mm, $z=220$ mm, $y=1$ (mm).

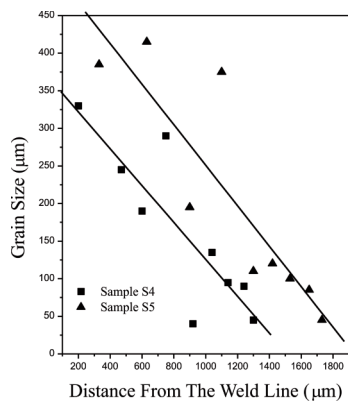


Figure 8. The measured grain size variation in HAZ, a) dissimilar joint, b) similar joint.

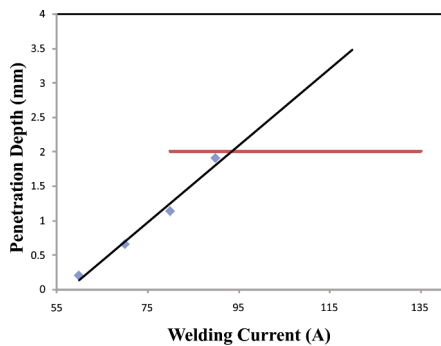


Figure 9. Variation of weld pool penetration depth vs. welding current.

5. Conclusions

In this work, a three-dimensional model was employed to predict thermal responses during similar and dissimilar gas tungsten arc welding of ferritic stainless steel. Also, welding experiments were conducted to evaluate the effect of welding current on grain size distribution in HAZ of the stainless steel side. The results show that:

In dissimilar joint due to the higher thermal

conductivity, carbon steel acts as a heat sink and consequently the higher amount of heat is transferred to carbon steel part. It results in smaller weld pool and the narrower HAZ of stainless steel in dissimilar weldments.

The grain size and its distribution are strongly dependent on the welding heat input. The sample with the highest welding current in similar weld (i.e. sample S6), shows larger grain size (about 450 μm), as well as more homogenous grain size distribution in the HAZ of AISI409.

The minimum welding current about 95A was obtained to achieve the full penetration for dissimilar joint. This welding current can be used to minimize the HAZ size and grain growth in dissimilar joint.

References

- [1] S. Kou, *Welding Metallurgy* 2nd edition, John Wiley & Sons, New Jersey, 2003.
- [2] D. E. Katsareas, A. G. Yostous, *Material Science Forum*, 490-491 (2005) 53-61.
- [3] E. Taban, A. Dhooge, E. Kaluc, *Materials and Manufacturing Processes*, 24 (2009) 649-656.
- [4] J. Choi, J. Mazumder, *Journal of Materials Science*, 37 (2002) 2143 - 2158.
- [5] G. Tsoukantas, G. Chryssolouris, *International Journal of Advanced Manufacturing Technology*, 35 (2008) 880 - 894.
- [6] T. Zakaria, S. A. David, J. M. Vitek, H. G. Kraus, *Metall Trans. B*, 22, (1991) 243-257.
- [7] C. H. Lee, K.H Chang, *Journal of Materials Science*, 42 (2007) 6607-6613.
- [8] N. A. McPherson, K. Chi, M. S. Mclean and T. N. Baker, *Materials Science and Technology*, 19 (2003) 219-226.
- [9] V.V. Satyanarayana, G. Madhusudhan Reddy, T. Mohandas, *Journal of Materials Processing Technology*, 160 (2005) 128-137.
- [10] C.H. Lee, K.H. Chang, C.Y. Lee, *Proceedings of the Institution of Mechanical Engineers, Part B: Journal of Engineering Manufacture*, 222 (2008) 1685-1694.
- [11] A.Hadadzadeh, M. M.Ghaznavi, A.H.Kokabi, *Materials and Design*, 125 (2014) 335-342.
- [12] E.Ranjbarnodeh, S. Weis, S. Hanke, A. Fischer, *J. Min. Metall. Sect. B-Metall.* 48 (1) B (2012) 115 - 121.
- [13] D. Priadi, R.A.M. Napitupulu, E.S. Siradj, *J. Min. Metall. Sect. B-Metall.* 47 (2011)199-209.
- [14] Z.Z. Zhang, C.S. Wu, *Computational Materials Science*, 65 (2012) 442-449.
- [15] M.Ohno, T.Yamaguchi, D.Sato, K.Matsuura, *Computational Materials Science*, 69 (2013) 7-13.
- [16] I. F. Fanous, M. Y. A. Younan, A. S. Wifi, *Trans. of ASME Journal of Pressure Vessels technology*, 125 (2003) 144-150.
- [17] J.N. Dupont, A.R.Mader, *Welding Journal*, (1995) 406-416.
- [18] F. F. Chung, P. S. Wei, *Journal of Heat Transfer*, 121 (1999) 451-61.
- [19] B. Taljat, B. Radhakrishnan, T. Zacharia, *Materials Science and Engineering A*, 246 (1998) 45-54.